Cupredoxin−Cancer Interrelationship: Azurin Binding with EphB2, Interference in EphB2 Tyrosine Phosphorylation, and Inhibition of Cancer Growth†

Anita Chaudhari, Magdy Mahfouz, Arsenio M. Fialho, Tohru Yamada, Ana Teresa Granja, Yonghua Zhu, Wataru Hashimoto, Beatrix Schlarb-Ridley, Wonhwa Cho, Tapas K. Das Gupta, and Ananda M. Chakrabarty*

Departments of Microbiology and Immunology, Surgical Oncology, and Chemistry, University of Illinois at Chicago, Chicago, Illinois 60612

Received August 15, 2006; Revised Manuscript Received November 8, 2006

ABSTRACT: Azurin is a member of a family of metalloproteins called cupredoxins. Although previously thought to be involved in electron transfer, azurin has recently been shown to preferentially enter cancer cells than normal cells and induce apoptosis in such cells. Azurin also demonstrates structural similarity to a ligand known as ephrinB2, which binds its cognate receptor tyrosine kinase EphB2 to initiate cell signaling. Eph/ephrin signaling is known to be involved in cancer progression. We now demonstrate that azurin binds to the EphB2-Fc receptor with high affinity. We have localized a C-terminal domain of azurin (Azu 96−113) that exhibits structural similarity to ephrinB2 at the G−H loop region known to be involved in receptor binding. A synthetic peptide (Azu 96−113) as well as a GST fusion derivative GST-Azu 88−113 interferes with the growth of various human cancer cells. In a prostate cancer cell line DU145 lacking functional EphB2, azurin or its GST-fusion derivatives had little cytotoxic effect. However, in DU145 cells expressing functional EphB2, azurin and GST-Azu 88−113 demonstrated significant cytotoxicity, whereas ephrinB2 promoted cell growth. Azurin inhibited the ephrinB2-mediated autophosphorlyation of the EphB2 tyrosine residue, thus interfering in upstream cell signaling and contributing to cancer cell growth inhibition.

Blue copper proteins, a subfamily of the monomeric cupredoxins, are low molecular weight (10−14 kDa), water-soluble proteins involved in the electron transport chain of prokaryotes and eukaryotes (*1*, *2*). We have previously shown that bacterial cupredoxins, such as azurin or rusticyanin, can enter mammalian cells and induce the inhibition of either cell cycle progression or apoptosis, leading to growth arrest or cell death (*3*−*5*). Recently, Yamada et al. (*6*) demonstrated that although rusticyanin could enter into both cancer and normal cells, azurin was proficient in entering human cancer cells but was deficient in entering normal cells. The preferential entry of azurin in cancer cells has been identified to be a domain with only 28 amino acids, designated Azu 50−77, that acts as a potential protein transduction domain (PTD[1]), which can be used as a vehicle to preferentially transport cargo proteins into cancer cells (*6*). After internalization, azurin forms a complex with the tumor suppressor protein p53, stabilizing it and increasing its intracellular level, thereby inducing apoptosis via caspase-mediated mitochondrial cytochrome *c* release pathways or cell cycle arrest at the G1 phase, depending on cell types (*4*, *7*). Rusticyanin has been reported to allow the mobilization of p53 to mitochondria, generating reactive oxygen species (ROS) and triggering apoptosis in cancer cells (*5*). In both cases, however, cell death and consequent inhibition of cancer cell progression was only partially p53-dependent, suggesting the possible involvement of a p53-independent pathway as well.

A large repertoire of structural data is available for several members of the cupredoxin superfamily, such as plastocyanin, azurin, auracyanin, pseudoazurin, rusticyanin, cucumber basic protein, and stellacyanin (*1*, *8*). The cupredoxins have an invariant β-sheet sandwich structure (Greek key beta-barrel), formed by seven or eight parallel and antiparallel strands, a variable α-helix region situated outside of the barrel, and a conserved mononuclear copper binding site (*8*). Amino acid sequence homology among these proteins, however, is only about 10% (*8*). During the past few years, it has become clear that cupredoxins exhibit remarkable topological similarity (having a common type of Greek key β-barrel) to a family of ligands called ephrins (*9*−*11*). Ephrins are eukaryotic proteins subdivided into two classes (A and B) based on their sequence homology; ephrinA1 to A8 are cell membrane-linked, whereas ephrinB1 to B6 possess highly conserved intracellular domains and a transmembrane domain. The ephrin ligands bind with a family of 14 extracellular receptor proteins known as Eph receptor tyrosine kinases (*12*). The Eph and ephrin proteins are present in distinct locations of their cells and have been shown to be up-regulated in many tumors (*13*). For example, EphB2 is up-regulated in glioblastoma (*14*), hepatocellular carcinoma

† This work was supported by a Sponsored Research Agreement between CDG Therapeutics and the University of Illinois at Chicago. A.M.F. acknowledges FEDER and Fundacao para a Ciencia e a Tecnologia (FCT), Portugal (grant POCTI/BIO/58401/2004). A.T.G. acknowledges a Ph.D. grant (BD/10328/2002) from Fundacao para a Ciencia e Tecnologia (FCT), Portugal.

* To whom correspondence should be addressed. Fax: 312-996-6415. E-mail: pseudomo@uic.edu.

[1] Abbreviations: FBS, fetal bovine serum; MTT, 3-(4,5-dimethylthiazol-2-yl-2,5-diphenyl tetrazolium bromide); PTD, protein transduction domain; SPR, surface plasmon resonance; ROS, reactive oxygen species.

10.1021/bi061661x CCC: $37.00
Published on Web 01/24/2007

(*13*), gastrointestinal cancers (*15*), prostate cancer (*16*), lung cancer, ovarian cancer, and renal carcinomas (*17*).

Crystal structures of the complexes between EphB2/ephrinB2 and EphB2/ephrinA5, revealed that the Eph receptor binds its cognate ephrin ligand with a 1:1 stoichiometry and nanomolar affinity through a heterodimerization interface (*9*−*11*). More specifically, the Eph receptor forms a cavity at the surface to accommodate the region of ephrin around the G−H loop (*9*−*10*). Upon Eph−ephrin complex formation, the Eph−ephrin heterodimerization subsequently leads to the trans autophosphorylation of the tyrosine kinase domains of the receptor molecules, allowing cellular signaling that translates into a variety of pathological processes, including tumor progression, angiogenesis, migration, and invasion related to many types of human cancers, Crohn's disease, chronic pain following tissue damage, inhibition of nerve regeneration after spinal cord injury, and human congenital malformations (*17*−*19*). It is also interesting to note that ephrin B2 was recently found to specifically bind to the attachment (G) glycoproteins of Nipah virus and Hendra virus to serve as a functional receptor for the entry of both viruses in a broad host of animals and humans (*20*, *21*).

Given the efficacy of azurin in promoting *in vitro* and *in vivo* cancer regression via p53-dependent and independent mechanisms (*3*, *4*, *7*), and as a consequence of its structural similarity with ephrin ligands (*10*), we proposed that cupredoxins might act as antagonists of Eph−ephrin mediated cell signaling and tumor progression. To address this issue, we have investigated the binding of cupredoxins with Eph receptors such as EphB2 and have assessed the functional consequences of these interactions. The data obtained provide the first experimental evidence that azurin and a C-terminal domain Azu 88−113 selectively bind to EphB2. Such binding of azurin with EphB2 leads to interference in the autophosphorylation of the tyrosine residue in its kinase domain in the presence of ephrinB2. Furthermore, an azurin peptide, synthesized on the basis of the structural similarity alignment with the high affinity binding G−H loop domain of ephrinB2, was able to induce cytotoxicity and cell growth inhibition in specific cancer cell lines, providing interesting clues to possible applications in cancer therapy.

EXPERIMENTAL PROCEDURES

Cell Culture. The human Glioblastoma LN 229 and MCF-7 (breast cancer) cells were cultured in RPMI medium 1640 containing 2 mM L-glutamine, 10 mM Hepes, 10% (v/v) heat-inactivated FBS, 100 units/mL penicillin, and 100 μg/mL streptomycin at 37 °C in a humidifier incubator with 5% CO_2 as described earlier (*6*, *22*).

Purification of Azurin and Plastocyanin. *Escherichia coli* JM109 and BL21 (DE3) were used as host strains for the hyperproduction of azurin, rusticyanin, and plastocyanin. Azurin and rusticyanin were purified as described previously (*3*, *5*). Construction and purification of GST−azurin fusion derivatives have been reported earlier (*6*). Purification and expression of plastocyanin from *Phormidium laminosum* was essentially carried out as described earlier (*23*), except that *E. coli* strain BL21(DE3)Cd+(RIL) was used instead of BL21(DE3). The concentration of fully oxidized protein was spectrophotometrically determined at 598 nm, using an extinction coefficient of 4700 M^{-1} cm^{-1}.

Construction of Expression Plasmids Encoding GST-Azu 88−*113 YMFF Motif Mutations*. Several mutations in the YMFF domain of GST-Azu 88−113 were generated using the Quick change site-directed mutagenesis kit (Stratagene, La Jolla, CA). The following primer pairs were used to generate such mutations: mutant 1, GST-Azu 88−113 YMAF, (FP:5′ AGGAAGGCGAGCAGTACATGGCCT-TCTGCACCTTCCCGGG3′, RP: 3′ TCCTTCCGCTCGTC ATGTAC CGGAAGACGTGGAAGGGCCC 5′); mutant 2, GST-Azu 88−113 AMFA (FP: 5′ AGGAAGGCGAGCAG-GCCATGTTCGCCTGCACCTTCCCGGG3′, RP: 3′ TC-CTTCCGCTCGTCCGGTACAAGCGGCGGAAGACGT-GGAAGGGCCC5′); mutant 3, GST-Azu 88−113 AMAA (FP:5′ AGGAAGGCGAGCAGGCCATGGCCGCCTGCA CCTTCCCGGG3′, RP:3′ TCCTTCCGCTCGTCCGGTAC-CGGCGGACGTGGAAGGGCCC5′); mutant 4, GST-Azu 88−113 AMAF (FP:5′ AGGAAGGCGAGCAGGCCATG-GCCTTCTGCACCTTCCCGGG3′, RP: 3′ TCCTTCCGCTC-GTC CGGAAGACGTGGAAGGGCCC5′). 10 ng of the GST-Azu 88−113 expression plasmid was used as a template in the site-directed mutagenesis quick change reactions with each of the primer pairs to generate specific mutants according to the manufacturer's instructions for 18 cycles. All of the mutations have been confirmed by sequencing, followed by expression of the mutant genes and protein purification.

Chemicals and Reagents. The Eph ectodomain Fc fusion proteins and ephrins were purchased as lyopholized powders from R & D Systems, Minneapolis, MN. All other chemicals used for surface plasmon resonance and growth experiments were purchased from Biacore AB International or Sigma and were of high analytical grade.

Peptide Design and Synthesis. Structurally based sequence alignment of azurin and plastocyanin with human ephrinB2 ectodomain was used to design peptides based on the region mediating the high affinity binding of ephrinB2 to the EphB2 receptor (G strand−loop−H strand of the ephrinB2-Fc ectodomain) of azurin, namely, Azu 96−113 (96-TFD-VSKLKEGEQYMFFCT-113). The peptide was purchased from GenScript Corporation, NJ as 99% pure. It was purified by reverse phase high-pressure liquid chromatography and its identity verified by mass spectrometry. Peptides were dissolved in phosphate-buffered saline (PBS) (1×) and stored as aliquots at −20 °C until use.

High Performance Size Exclusion Chromatography Studies. The commercially purchased Eph-Fc and ephrin-Fc proteins were characterized using a SuperSW3000 analytical TSK gel filtration column from Tosoh Biosciences attached to a Waters HPLC. Then, 200 μg/125 μL PBS protein solutions were injected (35 μL) onto the column equilibrated in PBS at a flow rate of 0.09 mL/min, and A_{280} nm was monitored for 60 min. Protein standards including IgG (126 kDa) and BSA (67.9 kDa) were used for calibration.

Surface Plasmon Resonance Analysis. Direct protein−protein interactions between cupredoxins or GST-peptides or their mutant forms with Eph-Fc were determined with a Biacore X biosensor system (Biacore AB), which is based on surface plasmon resonance (SPR) technology. In initial screening experiments, immobilization of azurin, rusticyanin, or plastocyanin to a single channel on the CM5 sensor chip was achieved using the amine coupling procedure. Sequential injections of *N*-hydroxysuccinimide/*N*-(3-dimethylamino-

propyl)-*N*-ethylcarbodiimide (0.05 M/0.2 M, 35 μL), cupredoxin protein (255 μM, 50 μL), 1 M ethanolamine (50 μL, pH 8.8), and 100 mM NaOH (10 μL) covalently linked the proteins to CM5 sensor chips with increases in resonance signals of 300 RU. Binding experiments were conducted via sequential injections of 100 nM Eph-Fc proteins in HBS-EP running buffer (0.01 M HEPES at pH 7.4, 0.15 M NaCl, 3 mM EDTA, and 0.005% v/v Surfactant P20) over the sensor surfaces at flow rates of 5 and 30 μL/min for 2.3 min (70 μL injection) with intermediate injections of 100 mM NaOH (10 μL pulse) to regenerate the cupredoxin−CM5 surface. All binding experiments were run against a bare Au CM5 sensor surface (negative channel) to correct for nonspecific binding.

Further studies examined the interactions of EphB2-Fc with azurin and GST-Azu peptides. Azurin or GST-Azu peptides were injected at increasing concentrations (0.05−100 nM) to EphB2-Fc or ephrinB2-Fc modified CM5 chips with 100 mM NaOH pulses in between injections. The data were fit to a Langmuir (1:1) binding model ($R_{eq} = R_{max}/(1 + K_d/C)$) to extrapolate equilibrium binding constants (K_d). The GST-Azu 88−113 mutants were titrated onto sensor chips immobilized with EphB2-Fc, EphA6-Fc, or EphA7-Fc, and the binding titrations were conducted via 50 μL injections of analyte.

Competition binding titrations were conducted in a manner similar to that of binding constant studies except that EphB2-Fc (246 nM) + competitor (azurin or GST-Azu (0−800 nM)) were injected over the ephrinB2-Fc−CM5 sensor surface.

Transfection, Immunoprecipitation, and Western Blotting. DU145 cells (ATCC) were maintained in RPM1 1640 medium with 10% heat-inactivated fetal bovine serum, 2 mM L-glutamine, and 100 units/mL penicillin/streptomycin (Life Technologies). EphB2 cDNA was obtained from Origene, Inc. Two micrograms of EphB2 DNA was transfected into DU145 cells in a 6 well plate using Lipofectamine 2000 and Opti-MEM medium (Invitrogen, Inc.). The cells were incubated for 48 h and serum starved for 6 h prior to ephrinB2 and azurin stimulation. Untransfected or transfected DU145 cells were treated with different concentrations of ephrinB2 and azurin or a combination of both. Cells were harvested and rinsed once in phosphate-buffered saline A and lysed in phospholipase C lysis buffer with 10 μg/mL aprotonin, 10 μg/mL leupeptin, 1 mM sodium vanadate, and 1 mM phenylmethylsulfonyl fluoride. Cell lysates were used for immunoprecipitation with 5 μg of EphB2 antibody (R&D Systems, Inc.). The immunoprecipitates were eluted by boiling in 2× SDS sample buffer, separated by SDS−polyacrylamide gel electrophoresis, and probed by immunoblotting with antiphosphotyrosine antibody (R&D Systems, Inc.). After incubation with horseradish peroxidase-conjugated anti-rabbit IgG antibodies (Amersham Pharmacia Biotech), anti-P-Tyr proteins were visualized with the enhanced chemiluminescence (ECL) detection system according to the manufacturer's instructions (Amersham Pharmacia Biotech). Quantification of the bands in the linear range of exposure was performed by densitometry using the NIH Image 1.54 software.

Cytotoxicity Assay. For the measurement of the cytotoxicity of the azurin synthetic peptide, the 3-(4,5-dimethylthiazol-2-yl-2,5-diphenyl tetrazolium bromide) (MTT) (Sigma) assay (*24*) was conducted. Approximately 2×10^4 cells per well were seeded into 96-well culture plates in 100 μL of RPMI 1640 medium. After growth overnight, the supernatant was removed, and new media containing azurin synthetic peptide at various specified concentrations were added to the attached cells. After 24 or 48 h of treatment, 10 μL of 5 mg/mL MTT solution was added to the culture and incubated for 1 h at 37 °C. The MTT reaction was terminated by the addition of 40 mM HCl in isopropanol. The MTT formazan formed was spectrophotometrically measured as described earlier (*24*). Untreated control cells were compared to treated cells to determine viability and, therefore, a measure of cytotoxicity.

Table 1: Structural Similarity of the EphrinB2 Ectodomain to Selected Cupredoxins with the Alignments to EphrinB2 (1KGY_E) Made Using VAST (*26*) and DALI (*25*) Algorithms

pdb	name	VAST score[a]	DALI Z score[b]	rmsd[c] to 1KGY_E	alignment length	% identity
1IUZ	plastocyanin	11.0	6.4	1.8	67	9.0
1JZG	azurin	10.1	6.7	3.4	90	5.6
1RCY	rusticyanin	9.7	6.1	3.1	87	8.0

[a] VAST score: the VAST structure-similarity score; this number is related to the number of secondary structure elements superimposed and the quality of the superposition. Higher VAST scores correlate with higher similarity. [b] DALI Z score: the Z scores are calculated using pairwise comparisons of the ephrin ectodomain structure with other structures in the DALI database. The higher the Z score, the less likely it is that the similarity between the 3D structures is random (pairs with $Z < 2.0$ are structurally dissimilar). [c] rmsd: Root-mean-square deviation of backbone residues in angstroms between the aligned parts of the pair of structures.

Computational Analysis. Structural similarities between the ephrinB2 ectodomain and cupredoxins were determined by using VAST and DALI algorithms (*25*, *26*), respectively, available at http://www.ncbi.nlm.nih.gov/Structure/VAST and http://www.ebi.ac.uk/dali/Interactive.html. Structure-based pairwise sequence alignments were calculated using the VAST algorithm. Protein structural diagrams are performed in two dimensions using TOPS (topology of protein structure) cartoons (*27*). The assessments of the structures were performed by using the program Mol Mol (*28*).

RESULTS

Structural Similarities between the EphrinB2 Ectodomain and Cupredoxins. As noted in previous structural studies (*9*, *10*) and defined by the SCOP database (structural classification of proteins; http://scop.mrc-lmb.cam.ac.uk/scop/), cupredoxins showed considerable topological similarity (having a common type of Greek key β-barrel) with ephrins, whose ectodomain is an eight-stranded β-barrel arranged in two sheets around a hydrophobic core (*9*−*11*). We used VAST and DALI programs (*25*, *26*) to search the 3D databases for structural homologues of the human ephrinB2 ectodomain. Several homologues were found with both programs (data not shown), including a small subset of monomeric cupredoxin proteins, plastocyanin, azurin, and rusticyanin. Specifically, the structural comparison between the ephrinB2 ectodomain and these three cupredoxins (which are chosen as representative proteins of the cupredoxin family) provided VAST and DALI alignments with significant and quite similar scores, respectively, ranging from 11.0 to 9.7 (out of a maximum possible 15.7) and 6.7 to 6.4. DALI Z scores <2.0 are structurally dissimilar (Table 1). The most notable

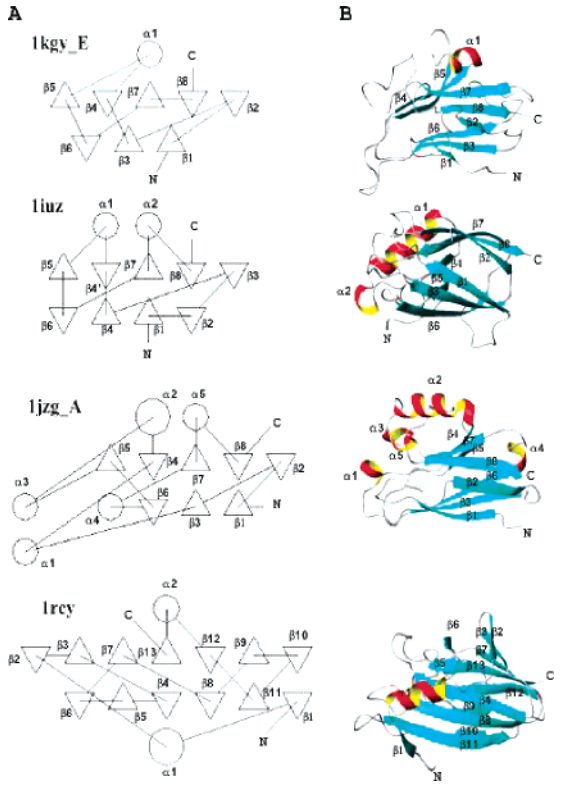

FIGURE 1: Comparison among the structures of the ephrinB2 ectodomain from humans (1kgy_E), plastocyanin from *Ulva pertusa* (1iuz), azurin from *Pseudomonas aeruginosa* (1jzg_A), and rusticyanin from *Thiobacillus (Acidithiobacillus) ferrooxidans* (1rcy). (A) The topology of each protein is shown using TOPS cartoons. TOPS cartoons represent the structure as a sequence of secondary structure elements (SSEs): β-strands (depicted as triangles) and helices (alpha and 3_{10}) (depicted as circles), their connection in a sequence from amino to carboxyl terminus, and their relative spatial positions and orientations. The direction of the elements can be deduced from the connecting lines. Up strands are indicated by upward pointing triangles and down strands by downward pointing triangles. (B) The Figures were drawn using the MolMol program (*28*).

structural conservation exists between the ephrinB2 ectodomain and plastocyanin, superimposed with a root-mean-square deviation (rmsd) of 1.8 Å (calculated over 67 structurally equivalent Cα atoms) (Table 1). In contrast, azurin, plastocyanin, and rusticyanin exhibit weaker primary sequence identity (less than 10%) with the ephrinB2 ectodomain (Table 1).

Figure 1 shows TOPS cartoons (A) and MolMol pictures (B) of the ephrinB2 ectodomain and each of the three cupredoxins under study. The topological description showed that the proteins adopt a sandwich of two β-sheets that form the core of the Greek-key fold and show remarkable structural similarity in the number and orientation of the β-strands; 1kgy_E, ephrinB2; 1iuz, plastocyanin; and 1jzg_A, azurin (Figure 1). In contrast, the number and arrangement of α-helices are much less conserved. In jzg A, the helical structure co-incident with the protein transduction domain (PTD) (α2 and α3 in Figure 1) responsible for preferential entry into cancer cells versus normal cells (*6*) is unique compared with that of the other proteins represented herein. As can be expected for proteins with different sizes, the loops that connect the elements of secondary structure showed differences in their lengths and conformations. It is also noteworthy that 1rcy (rusticyanin) has the lowest structural homology, with substantial differences in the lengths of shared secondary structure elements (SSEs) and the presence of non-shared SSEs.

In summary, the remarkable structural similarity between cupredoxins and ephrin extracellular domains poses an interesting question: Can cupredoxins, in particular plastocyanin and azurin, act as antagonists in preventing ephrin binding with the Eph family of receptor tyrosine kinases, thereby interfering with the ephrin signaling system and preventing cancer progression? This question is particularly pertinent to azurin because purified azurin was shown not only to preferentially enter cancer cells than normal cells (*6*) but also to induce apoptosis and *in vivo* regression of melanoma and breast cancers (*3*, *4*). We, therefore, investigated by using a series of *in vitro* binding experiments whether azurin and plastocyanin can interact specifically with Eph receptors or their ligands.

Analysis of Eph-Fc Receptor−Cupredoxin Interactions. Specific interactions of the Eph receptors with cupredoxins were determined by surface plasmon resonance (SPR) analyses, and the data are represented in Figure 2. Before conducting such studies, we determined the oligomerization status of the purified Eph receptor and ephrin ligand proteins by high performance size exclusion chromatography as described under Experimental Procedures. The data showed that the proteins remained in the monomeric state (Table 2). SPR sensorgrams for the binding of immobilized cupredoxins with Eph-Fc indicated selective recognition between these two subsets of proteins (Figure 2A−C). In these measurements, Eph-Fc concentrations were kept constant at 100 nM so that the differences in the degree of association expressed in terms of R_{eq} reflect the differences in affinities between the Eph-Fc receptor proteins and cupredoxins. Azurin showed the highest affinity for EphB2-Fc and A6 and also tightly bound A4 and A7 (Figure 2A). However, plastocyanin showed selectivity for EphA1-Fc, A3 and B2, and, to a lesser degree, A2 and A6 (Figure 2B). Finally, rusticyanin recognized EphA8-Fc and B1, but only weakly (Figure 2C). The associative interactions of azurin with EphB2-Fc and EphA6-Fc were the highest with R_{eq} values 1248 and 1200 RU, respectively. The cross-selectivities of the cupredoxins for EphA-Fc and EphB-Fc receptor subfamilies are not unprecedented because the interactions of EphB2-Fc/ephrinA5-Fc, EphA4-Fc/ephrinB1-Fc, and EphA4-Fc/ephrinB2-Fc have been reported (*29*, *30*). Perhaps the most interesting finding is that azurin has high affinity for EphB2-Fc in that both of these proteins have been reported to be involved in cancer cell signaling, cancer cell death, or in cancer progression (*3*, *4*, *6*, *17*). We, therefore, investigated the interactions of azurin with EphB2-Fc in further detail.

Binding Affinities of Azurin and GST-Azu Peptides with EphB2-Fc. SPR binding measurements were performed with azurin or GST-Azu peptides using the immobilized EphB2-Fc to evaluate the relative binding affinity of the full length azurin or its various domains for the EphB2-Fc receptor. Our experimental strategy for elucidating the structural determinant of azurin for EphB2-Fc binding is shown in Figure 3, which depicts the map of the primary/secondary structural parameters of azurin and the GST-Azu constructs as described earlier (*6*). In particular, the GST-Azu 88−113 is coincident with the G−H loop region of ephrinB2-Fc (native ligand), and therefore, its binding efficacy with EphB2-Fc

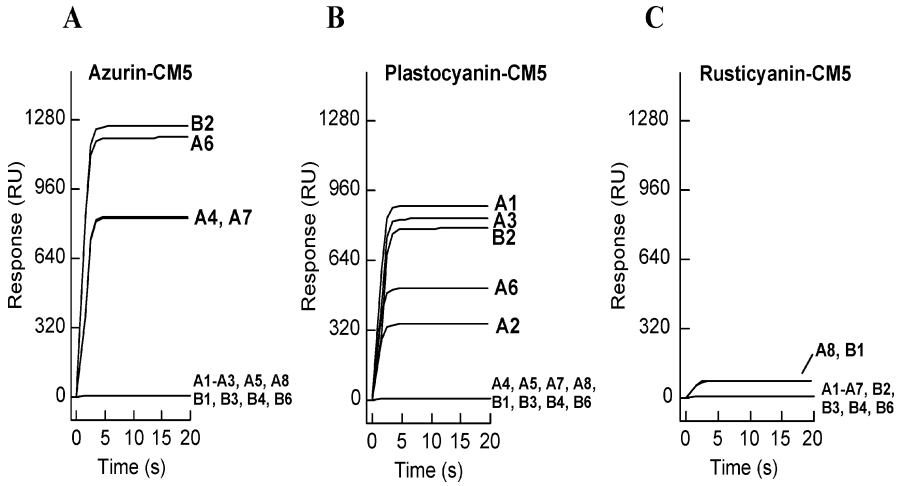

FIGURE 2: Surface plasmon resonance sensorgrams for the association of cupredoxins with Eph-Fc. Selective binding of azurin (A), plastocyanin (B), and rusticyanin (C) with EphA-Fc and EphB-Fc proteins. The binding screens were conducted on cupredoxin modified sensor chips with sequential injection of 100 nM Eph-Fc receptors at a flow rate of 30 μL/min over 2.3 min. The curves represent the beginning of the association phase for the interactions of Eph-Fc with azurin, plastocyanin, and rusticyanin. Relative binding trends were taken as a function of the saturating resonances (R_{eq}), which varied from 79 RU for rusticyanin binding to EphB1-Fc or EphA8-Fc to 1248 RU for azurin binding to EphB2-Fc. The cross-selective binding of cupredoxins to specific EphA and EphB receptor proteins is notable with the best interactions occurring between cupredoxin and EphB.

Table 2: High Performance Size Exclusion Chromatographic Characterization Data for Eph and Ephrin Receptors[a]

protein	monomer MW (kDa)	glycosylated monomer MW (kDa)	retention time (min)	calculated MW (kDa)	oligomerization state
EphB2-Fc	85.3	100−110	11.8	88.562	monomer
EphA6-Fc	86.0	100	11.5	91.502	monomer
EphA7-Fc	85.7	110	11.1	95.423	monomer
ephrinB2-Fc	49.6	60−65	14.0	67. 000	monomer
ephrinA1-Fc	46.8	50−55	14.5	62.099	monomer

[a] The details of this characterization are given in Experimental Procedures.

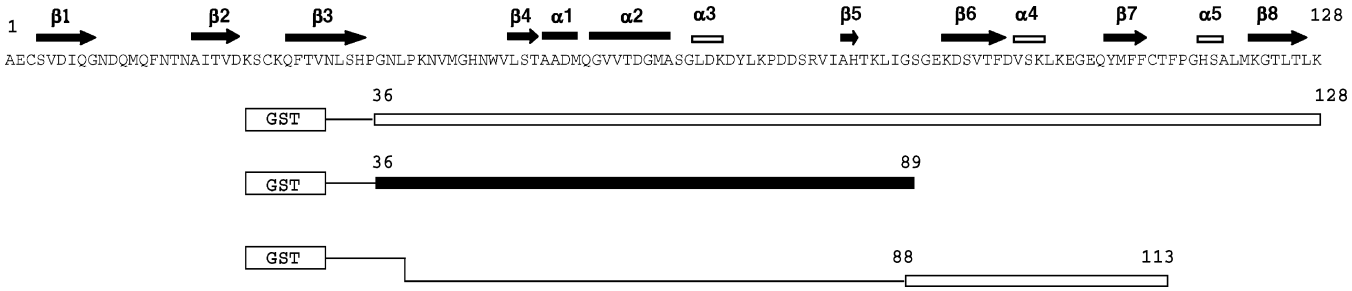

FIGURE 3: Schematic representation of various truncated azurin constructs derived from full length azurin. Secondary structure elements are illustrated as arrows for β-sheets and as rectangles for helices (alpha and 3_{10}). Various segments of the gene encoding the 128 amino acid azurin were fused at the 3′-end of the *gst* gene (encoding glutathione S-transferase) in frame, cloned in *E. coli*, hyperexpressed, and the fusion proteins purified as described earlier (*6*).

was of particular interest. Initial binding measurements of azurin and various GST-Azu constructs (all at 100 nM) for EphB2-Fc revealed their relative affinity, that is, azurin > GST-Azu 88−113 > GST-Azu 36−128 > ephrinB2-Fc > GST-Azu 36−89 ≫ GST (Figure 4A). To quantify the binding affinities, the saturating response values (R_{eq}) for azurin or GST-Azu were measured as a function of their concentrations (0−100 nM) (Figure 4B). The binding data were fit to a simple Langmuir (1:1) binding equation (described in Experimental Procedures) to determine equilibrium dissociation constants (K_d). Notably, azurin (K_d = 6 nM) and GST-Azu 88−113 (K_d = 12 nM) had 5- and 2.5-fold higher affinities, respectively, for EphB2-Fc than its native ephrinB2-Fc ligand (K_d = 30 nM). Also, GST-Azu 36−128 (Table 3) showed a slightly higher affinity (K_d = 23 nM) than ephrinB2-Fc (K_d = 30 nM). In contrast, GST-Azu 36−89 and GST exhibited negligible binding (Table 3). These data indicate the significance of the Azu 88−113 region of azurin for high affinity EphB2-Fc interaction. The Azu 88−113 region consists of the G−H loop domain that is structurally homologous to the G−H loop found in ephrinB2. Such a peptide may thus be a potential antagonist in EphB2/ephrinB2 signaling. We, therefore, performed *in vitro* and *in vivo* competition assays to explore this possibility.

Competition Binding Studies for Azurin/GST-Azu and EphrinB2-Fc with EphB2-Fc. To better understand the physiological effects of high-affinity azurin-EphB2-Fc binding, we performed a SPR analysis of binding of EphB2-Fc to ephrinB2-Fc immobilized onto a CM5 sensor chip after

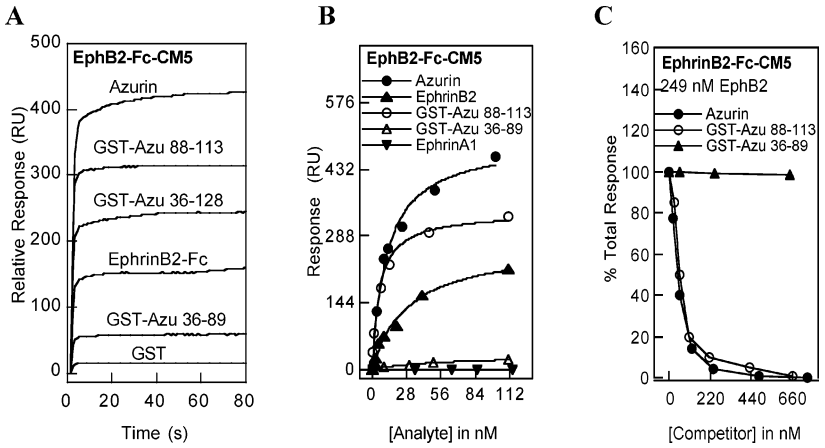

FIGURE 4: SPR binding titrations depicting the interactions of azurin and GST-Azu constructs with immobilized EphB2-Fc or immobilized ephrinB2-Fc. (A) An initial screening experiment was performed to determine the relative binding of azurin or GST-Azu wherein the SPR traces were recorded after injection of the cupredoxins (100 nM) onto EphB2-Fc-modified CM5 sensor chips. (B) Binding affinity curves for the interactions of azurin, GST-Azu 88−113, ephrinB2-Fc, GST-Azu 36−89, and ephrinA1-Fc to the immobilized EphB2-Fc after titrating increasing concentrations (0.05−112 nM) of the cupredoxins. Binding dissociation constants (K_d) were calculated (Table 3) after fitting the data to a Langmuir (1:1) binding model using the equation $R_{eq} = R_{max}/(1 + K_d/C)$. (C) Binding competition with ephrinB2-Fc immobilized on CM5 sensor chips. Azurin (or GST-Azu) + EphB2-Fc samples were added at different azurin concentrations (0−800 nM, [ephrinB2-Fc] is 249 nM) to the sensor surface, and the data were plotted as a ratio of resonances, % total response (R_{eq} (azurin + EphB2-Fc)/(R_{eq}/(EphB2-Fc))).

Table 3: Relative Binding Affinities of Azurin and GST-Azu Constructs with EphB2-Fc

analyte	R_{eq} in RU[a]	MW	K_d in nM[b]
wt azurin	427	13,929	6 ± 0.75
ephrinB2-Fc	159	65,100	30 ± 5.1
GST	14	26,000	>10,000
GST-Azu 36−128	244	36,076	23 ± 1.5
GST-Azu 36−89	57	31,924	>1000
GST-Azu 88−113	314	28,943	12 ± 1.5

[a] The data from an initial screening experiment were generated upon injection of 100 nM analyte to the sensor surfaces, and the saturating signals (R_{eq}) are listed in resonance units. [b] Saturation in binding was achieved at each titration point in the binding curves depicted in Figure 4B, and these values plotted against [analyte] were used to calculate equilibrium dissociation constants (K_d).

EphB2-Fc is incubated with varying concentrations of azurin and GST-Azu constructs. Figure 4C shows the inhibition of EphB2-Fc ([EphB2-Fc] = 249 nM) binding to ephrinB2-Fc by 0−800 nM azurin, GST-Azu 88−113, and GST-Azu 36−89. The inhibition is expressed in terms of % total response (= (R_{eq} azurin + EphB2-Fc)/R_{eq} (EphB2-Fc alone)) × 100. The inhibition profiles indicate diminished binding of total protein to the immobilized ephrinB2-Fc when EphB2-Fc is preincubated with azurin or GST-Azu 88−113 with azurin being a slightly more potent inhibitor than GST-Azu 88−113 (±10%). The preincubation of azurin or GST-Azu 88−113 with EphB2-Fc reduced total protein binding to the surface by up to 99% at stoichiometric and/or excess concentrations of the competitor. GST-Azu 36−89, however, did not affect total protein binding (Figure 4C), which is consistent with its weak binding to EphB2-Fc. It appears that azurin (or GST-Azu 88−113) forms a stoichiometric complex with EphB2-Fc because maximal inhibition was achieved with a 1:1 ratio of ephrinB2-Fc and azurin (or GST-Azu 88−113). Collectively, the binding data indicate that azurin has high affinity for EphB2-Fc and that it can interfere with ephrinB2-Fc−EphB2-Fc binding by competition with immobilized ligand ephrinB2 binding and receptor occupation.

Azurin Selectivities for EphA versus EphB Receptors Using GST-Azu 88−113 Mutants. In order to elucidate the recognition of azurin with various Eph receptors, mutant GST-Azu 88−113 constructs in which a consensus amino acid sequence YMFF having structural similarity alignment with the ephrinB2 recognition motif for EphB2 were prepared with the following designations: wild type (wt, YMFF), mutant 1 (M1, YMAF), mutant 2 (M2, AMFA), mutant 3 (M3, AMAA), and mutant 4 (M4, AMAF), and their interactions with various A and B type Eph receptors were determined in SPR studies. Figure 5A shows the binding titrations upon injections of increasing concentrations of GST-Azu 88−113 or M1−M4 onto immobilized EphB2-Fc, and Table 4 summarizes the extrapolated K_d values. The binding affinities decreased in the order wt (GST-Azu 88−113) or M1 > ephrinB2-Fc > M2, M4 ≫ M3 with the K_d values ranging from 12 ± 2.2 nM (wt and M1) to 63 ± 8.2 nM (M2 and M4). M3 exhibited no affinity in the nanomolar range for EphB2-Fc. These data suggest that one or both mutations in the terminal aromatic residues of the consensus YMFF sequence of azurin (mutants M2 and M4) can be tolerated with reduced binding affinity but the loss of all three aromatic residues (mutant M3) leads to a total loss of EphB2-Fc affinity.

To address the issues of the cross-selectivity of azurin with EphA and EphB receptors (both of which exhibited interactions with native azurin, Figure 2A), SPR binding analyses of immobilized EphA6 and immobilized EphA7 with GST-Azu 88−113 and M1−M4 were tested. Figures 5B and C show that the binding curves for wild-type GST-Azu 88−113 and M1 as well as the binding titration for a positive control ephrinA1-Fc could be generated, although the affinity of the M1 mutant was lower than that of the wt for both EphA6 and EphA7. Table 4 summarizes the calculated binding constants with EphA6 interactions of 7.93 ± 0.86 nM (wt), 7.8 ± 1.6 nM (ephrinA1-Fc), and 146 ± 10 nM (M1) and EphA7 interactions of 26.7 ± 2.7 nM (wt) and 100 ± 5 nM (M1). Interestingly, M2, M3, or M4 could not recognize EphA receptors at nanomolar concentrations,

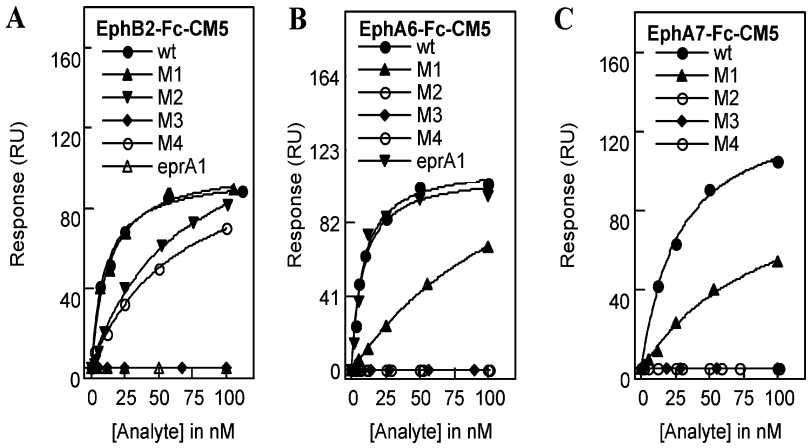

FIGURE 5: SPR binding titrations for the interactions of GST-Azu 88−113 and the YMFF mutants with EphA and EphB receptors. (A) SPR binding titrations of immobilized EphB2-Fc in contact with varying concentrations (0−100 nM) of GST-Azu 88−113 (wt), M1−M4 mutants, or ephrinA1 (eprA1). (B) and (C) Similar binding titration curves upon injection of GST-Azu 88−113 or its M1−M4 mutants with immobilized EphA6-Fc or EphA7-Fc. The curves represent the fits of the data to the Langmuir (1:1) binding model $R_{eq} = R_{max}/(1 + K_d/C)$ and are summarized in Table 4. Not all of the ligand bindings are shown above, but the K_d values are reported in Table 4.

Table 4: Binding Constants between Mutant GST-Azu 88−113 YMFF Fusions and A and B Type Ephs

	K_d (EphB2) nM	K_d (EphA6) nM	K_d (EphA7) nM
wild type (YMFF)	12.3 ± 2.2	7.93 ± 0.86	26.7 ± 2.7
mutant 1 (YMAF)	13 ± 1.6	146 ± 10	100 ± 5.0
mutant 2 (AMFA)	63 ± 8.2	0	0
mutant 3 (AMAA)	0	0	0
mutant 4 (AMAF)	63.3 ± 9.0	0	0
ephrinA1	0	7.8 ± 1.6	not measured
ephrinB2	30 ± 5.1	0	0

suggesting that the loss of even a single terminal aromatic amino acid (M4), which still allows binding with EphB2 at a lower affinity, strongly interferes in the binding of the azurin peptide with the A type receptors. The replacement of two terminal aromatic amino acids with alanine (M2) allows reduced binding of the mutant azurin with the EphB2 receptor but significantly reduces binding with the A type receptors.

Azurin and GST-Azu 88−113 Interfere with Tyrosine Phosphorylation at the Receptor−Tyrosine Kinase Domain of EphB2. Because azurin binds to EphB2 with high affinity and appears to compete with ephrinB2 for such binding, a pertinent question is whether azurin binding to EphB2 may allow the same level of tyrosine autophosphorylation in the absence or presence of ephrinB2. We used prostate cancer cell line DU145 with a truncating mutation in EphB2 and a deletion in the remaining allele (*31*). The DU145 cell line has a hemizygous nonsense mutation that results in the amino acid change Q723X truncating EphB2 at the kinase domain, leading to the loss of tyrosine phosphorylation and receptor signaling (*31*). Incubation of DU145 cells, either alone or in the presence of various concentrations of azurin, did not show the presence of either phosphorylated tyrosine or EphB2 (data not shown). Serum-starved DU145 cells, transfected with EphB2 cDNA with about 55% transfection efficiency, showed the presence of EphB2 protein, as demonstrated by Western blotting with anti-EphB2 antibody (Figure 6A, bottom panel, lane 2). Although there was no tyrosine phosphorylation in the absence of its ligand (Figure 6B, top panel, lane 3), the addition of increasing amounts of azurin allowed increasing phosphorylation of the tyrosine

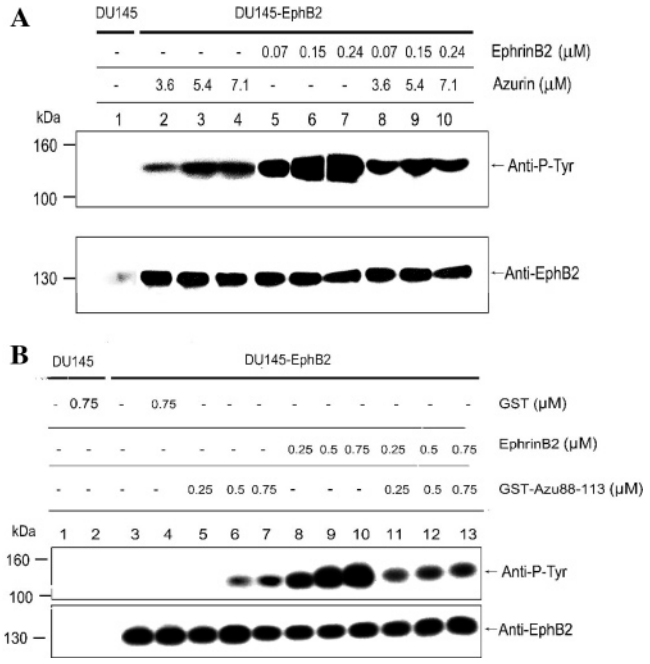

FIGURE 6: Response of DU145 cells, transiently expressing EphB2, to azurin and ephrinB2 treatments. (A) DU145 cells were serum starved and treated with different concentrations of azurin and ephrinB2 or a combination of both as shown. The lysates were immunoprecipitated with EphB2 antibody, and the immunoprecipitates were electrophoresed and blotted against anti-P-Tyr (upper panel) and with anti-EphB2 antibody (lower panel). (B) Treatment of DU145 cells (serum starved) with purified glutathione-S-transferase (GST), ephrinB2-Fc, GST-Azu 88−113 fusion construct, or a combination of ephrinB2 and GST-Azu 88−113. Cell lysates were immunoprecipitated, separated on the gel, and stained with anti-P-Tyr as conducted in (A).

residue, albeit at rather high concentrations (Figure 6A, top panel, lanes 2, 3, and 4). There was very little tyrosine phosphorylation even at 1.0 μM concentration of azurin (data not shown) as contrasted with 0.07 μM ephrin B2 (Figure 6A, lane 5, top). This suggested that the binding of azurin with the EphB2 receptor allowed very weak tyrosine phosphorylation in the absence of the ligand ephrinB2. In contrast, significant phosphorylation of the tyrosine residue was observed at lower concentrations of ephrinB2 (Figure 6A, top panel, lanes 5, 6, and 7). Most interestingly, a mixture

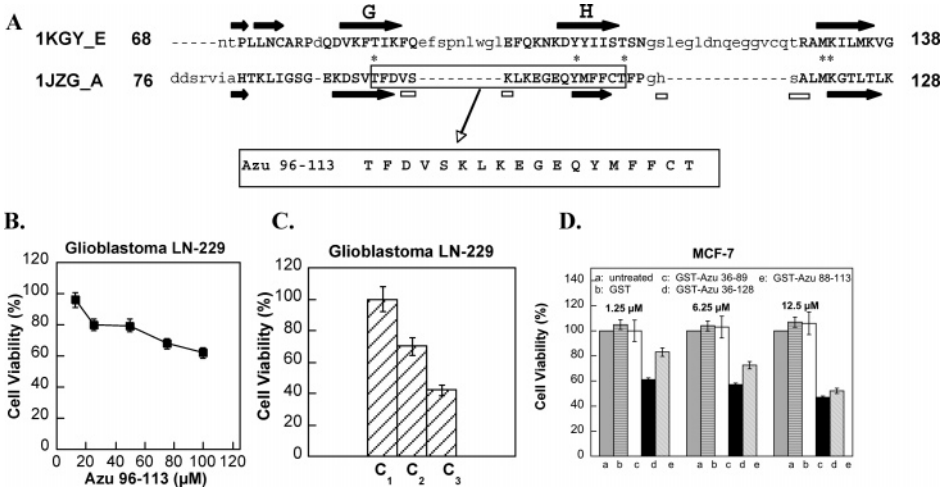

FIGURE 7: (A) Structural alignment comprising the C-terminal domains of azurin from *P. aeruginosa* (1jzg_A) with the human ephrinB2 ectodomain (1kgy_E) as computed by the VAST algorithm. Superimposed secondary structure elements are denoted by a bold capital letter. Dashes and lower-case lettering indicate areas where there are no alignments. Secondary structure elements according to the structures are illustrated as arrows for β-sheets and as open rectangles for 3_{10} helices. Identical amino acids are indicated by an asterisk. The azurin peptide (Azu 96−113), corresponding to the G−H loop region of ephrinB2, which is the main region mediating high affinity binding of the ephrins to the Eph receptors, is boxed and represented below each alignment. The G and H loop regions are marked with thick arrows on top of the amino acid sequences of ephrinB2. (B) Cytotoxic activity of Azu 96−113 synthetic peptide toward Glioblastoma LN-229 cells. Cytotoxicity effects were determined by MTT assay as described in Experimental Procedures. Percent cell viability is expressed as percentage of live cells compared to that of the untreated control (100% viability). (C) Cytotoxicity effects of Gellan gum (Gelrite) (C1), Azu 96−113 synthetic peptide (C2), and Azu 96−113 peptide−gellan gum mixture (C3) toward Glioblastoma LN-229 cells. (D) Effect of GST-Azu 36−128 and GST-Azu 88−113 on the viability of MCF-7 breast cancer cells. GST-Azu peptides were added at increasing concentrations (1.25, 6.25, and 12.5 μM) into 96 well plates containing 8×10^3 cancer cells per well, incubated at 37 °C for 48 h, and subsequently analyzed using the MTT assay (Experimental Procedures).

of azurin and ephrinB2 demonstrated a lower level of tyrosine phosphorylation (about 30−40%; compare lanes 5, 6, and 7 with lanes 8, 9, and 10), indicating a strong *in vivo* interference of EphB2−ephrinB2-mediated cell signaling by azurin. Similar experiments were conducted with GST-Azu 88−113 because of its high affinity interaction with EphB2 (Figure 4B). GST-Azu 88−113 stimulates tyrosine autophosphorylation in EphB2 transfected DU145 in the absence of ephrinB2 (Figure 6B, top panel, lanes 5, 6, and 7) but only at concentrations of 0.5 μM or higher. The levels of phosphorylation are much lower, however, compared to when ephrinB2 is added at the same concentrations (Figure 6B, top panel, lanes 8, 9, and 10). GST-Azu 88−113 activity is modulated by the Azu 88−113 sequence because GST alone showed no observable stimulation (Figure 6B, top panel, lane 4). Upon the cotreatment of EphB2 transfected DU145 cells with GST-Azu 88−113 and ephrinB2, EphB2 kinase domain tyrosine autophosphorylation was attenuated in a dose dependent manner (Figure 6B, top panel, lanes 11, 12, and 13). Statistically significant decreases in phosphotyrosine levels were determined (21, 42, and 45% for lanes 11, 12, and 13, respectively, as a function of intensities of lanes 8, 9, and 10). These results clearly demonstrate that azurin or Azu 88−113 competes with ephrinB2 to interfere in EphB2-associated cell signaling.

Does Azurin Binding to EphB2 Have Functional Significance? Because we now have knowledge of the region of azurin binding to EphB2 (Figure 4) and of its ability to interfere with the Eph receptor signaling system (Figure 6), it is now possible to design small truncated versions that might mimic the activity of azurin and its interference with the ephrin signaling system. Therefore, we purchased a chemically synthesized azurin peptide (Azu 96−113) in order to determine its capability to cause cytotoxicity toward cancer cells. We chose the peptide on the basis of the binding affinities of the GST-azurin derivatives/EphB2 receptor (Figure 4) and coincident with the X-ray crystallographic investigations of the EphB2−ephrinB2 complex (*9*, *10*). Thus, upon the structure-based sequence alignment of azurin and the human ephrinB2 ectodomain, we designed the peptide corresponding to the G−H loop region of ephrinB2 (called Azu 96−113), which is the main region mediating the high affinity binding of ephrins to the Eph receptors (*9*, *10*). In Figure 7A, the structural superimposition of the C-terminal segments of the ephrinB2 ectodomain and azurin can be seen.

Cytotoxic Activity of Azu 96−113 Synthetic Peptides and GST-Azu Fusion Derivatives toward Various Cancer Cell Lines. The Eph/ephrin signaling system is known to be involved in many pathological processes, such as cancer progression, inhibition of nerve regeneration following spinal cord injury, congenital malformations, and tissue-damage-induced triggering of pain (*12*, *17*, *32*). Consequently, successful attempts have been made in designing and identifying by phage display synthetic peptides that selectively bind to a single Eph receptor, or a limited number of receptors, thus acting as antagonists (*33*, *34*). Indeed, sequence optimization of one of the EphB4-binding peptides yielded an antagonist peptide with affinity comparable to that of an ephrin ligand (*34*). The ability of wt azurin or GST-Azu 88−113 to bind the EphB2-Fc receptor with an affinity higher than the ligand ephrinB2-Fc (Figure 4) suggests that during the course of natural evolution, bacteria have already evolved proteins with structural similarity to certain ephrins that make them or the peptides derived from them possessing the structural identity potent antagonists to the Eph/ephrin-mediated signaling process (Figure 6). In order to see if such domains of azurin may also play a role

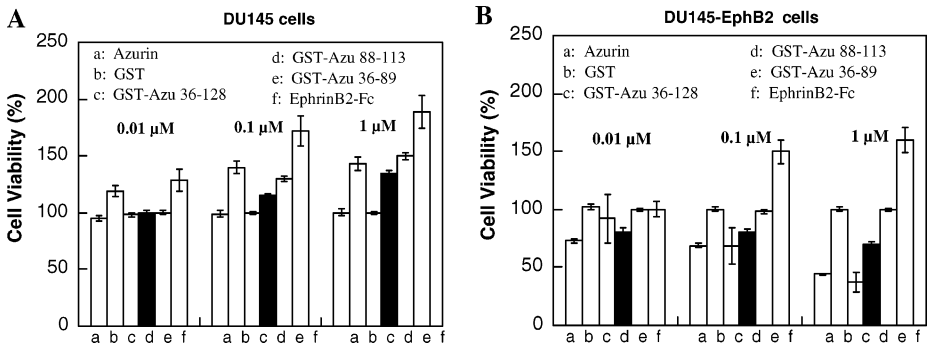

FIGURE 8: Effects of azurin and GST-Azu fusions on the growth of DU145 prostate cancer cells in the absence and presence of functional EphB2. (A) DU145 cells cultured in RPMI media in 96 well plates (1×10^4 cells/well) were treated with increasing concentrations of azurin, GST, GST-Azu fusions, or ephrinB2-Fc (0.01−1 μM) and were incubated for 48 h at 37 °C in 5% CO_2 atmosphere. The MTT assay was conducted as described in Experimental Procedures after 4 h of incubation with the MTT reagent, and the cell viability was determined spectrophotometrically. (B) DU145 cells transfected with functional EphB2 DNA were plated in wells to which were added varying concentrations of azurin, GST-Azu, or ephrinB2 and the MTT assay conducted as for the untransfected cells described above. Cell viability is calculated as a function of untreated cells and reported in terms of percentage. Standard deviations in general varied from 1 to 5%.

as antagonists to Eph signaling in cancer progression, we performed quantitative MTT assays in a number of cancer cell lines normally known to hyperexpress EphB receptors/ephrin ligands. Indeed, increasing concentrations of Azu 96−113 synthetic peptide led to reduced cell viability in glioblastoma LN-229 cells (Figure 7B).

One of the problems of using peptides is that they often lose their structures in solution and become less effective in targeting tumor cells. Certain polysaccharides are widely used in the pharmaceutical industry for the sustained release of drugs and as carriers to deliver protein- and peptide-based anticancer drugs (*35*). We have extensively studied the biosynthesis of one such polysaccharide, gellan gum (*36*), which is approved in the US and EU for use as gelling and suspending agents in food. A commercial preparation, Gelrite, is also used in the pharmaceutical industry as capsules for drug delivery (*37*). We, therefore, tested the ability of Gelrite to stabilize the Azu 96−113 peptide and promote its cancerocidal property. At 0.05 mg/mL, Gelrite had very little cytotoxicity toward glioblastoma LN-229 cells (Figure 7C, C1) but significantly enhanced the cytotoxicity of the 75 μM Azu 96−113 peptide (Figure 7C, C2) when used in combination (Figure 7C, C3), demonstrating its usefulness in potential bacterial peptide-based cancer therapy and perhaps in the treatment of other pathological conditions triggered by the Eph−ephrin signaling system.

We have also tested the ability of GST-Azu fusion peptides to induce cell growth inhibition in breast cancer MCF-7 cells. There was very little inhibitory effect (Figure 7D) triggered by GST or GST-Azu 36−89 fusion protein similar to that of the control (without protein treatment). However, GST-Azu 36−128 or GST-Azu 88−113, harboring the azurin region capable of interfering in ephrinB2/EphB2 binding, showed significant growth inhibition in a dose dependent manner (Figure 7D), confirming the role of the Azu 88−113 region in triggering MCF-7 cell growth inhibition.

Although the results in Figure 7B, C, and D demonstrate the role of azurin or its truncated derivatives (Azu 88−113, Azu 36−128) in imparting cytoxicity *in vitro* in cancer cells, we were also interested in knowing if azurin or its truncated derivatives would exert such an effect *in vivo* in cancer cells. To determine the effect of azurin or its peptides on DU145 cancer cell growth and a functional role of EphB2-mediated cell signaling, we incubated both DU145 and DU145 expressing functional EphB2 (DU145-EphB2) cells with azurin, GST, ephrinB2, and GST-Azu fusion proteins at three different concentrations (0.01, 0.1, and 1.0 μM) for 48 h and measured cell survival by MTT assays. None of these proteins demonstrated any cytotoxicity in EphB2-negative DU145 cells under such conditions, although GST, ephrinB2, and some GST-Azu fusions showed some growth stimulation at higher concentrations (Figure 8A). In contrast, azurin, GST-Azu 36−128, and GST-Azu 88−113 showed significant growth inhibition in EphB2-positive DU145 cells in a dose dependent manner, whereas ephrinB2-Fc showed stimulation of cell growth (Figure 8B), demonstrating the role of EphB2/ephrinB2-mediated cell signaling in prostate cancer cell progression and azurin or Azu 88−113 peptide-mediated inhibition of such cancer cell progression.

DISCUSSION

The role of ephrins and Eph receptors, which are known to be hyperexpressed on a variety of solid tumors and tumor cell lines, is well known for enhanced cancer progression (*17*, *38*). Null mutations in various ephrin/Eph gene families are also known to result in defects in vascular remodeling, leading to the conclusion that blocking ephrin/Eph receptor interaction could interfere with neovascularization of tumor tissue and consequently tumor growth (*39*). It is also interesting to note that ephrinB/EphB2 signaling directly induces subventricular germinal zone (SVZ) proliferation, decreases migration, and promotes SVZ neurogenesis (*40*). Migrating glioblastoma cells have been shown to overexpress EphB2 *in vitro* and *in vivo*, and thus, glioma migration and invasion are promoted by activation of EphB2 or inhibited by blocking EphB2 (*14*). The ability of the azurin peptide to induce cell death in glioblastoma cells (Figure 7B, C) or the ability of the GST-Azu 88−113 peptide to trigger cell death in MCF-7 cells (Figure 7D) can thus be ascribed to interference in EphB2 signaling. More interestingly, clinicopathological and survival correlation studies indicated statistically significant overall negative survival and shorter disease free survival with increased EphB2 expression among 94 breast carcinoma and 4 breast carcinoma cell lines (*41*), demonstrating a role of EphB2 in breast cancer cell proliferation.

Given the fact that azurin or the peptides derived from azurin that can bind strongly to the EphB2 receptor interfere

in the ephrin/Eph signaling system, it appears that such an interference most likely contributes, at least to some degree, to the known effect of azurin to induce cell death and *in vivo* regression of human breast cancer and melanoma in nude mice (*3*, *4*). Because azurin also binds relatively strongly with other Eph receptors, such as EphA6, EphA4, or EphA7 (Figure 2A), it is likely that azurin may interfere in signaling systems mediated by these A-type receptors as well, although the physiological significance of such interference remains to be deciphered. Some of the EphB receptor binding peptides identified earlier by phage display studies showed selective binding to a few receptors of A-class (*33*), and several of these EphA receptor binding peptides, similar to the G−H loop of A-class ephrins, were shown to harbor the motif ΩXXΩ, where Ω is an aromatic amino acid, and X is a nonconserved amino acid (*34*). It is thus interesting to note that the G−H loop region of azurin also harbors such a motif (YMFF in Azu 96−113, Figure 7A). Indeed, replacement by alanine of either one or both of the terminal aromatic amino acids of this motif modestly reduced azurin's binding to EphB2 but significantly reduced its binding affinity with the EphA6 or EphA7 receptors (Figure 5, Table 4). Although previously believed to be involved only in electron transfer during denitrification by *Pseudomonas aeruginosa*, mutational studies did not show any such role of azurin (*42*), and it now appears that azurin might function more as a modulator of host pathological conditions mediated both by the p53 tumor suppressor (*7*, *43*) and by the ephrin/Eph signaling system.

The ability of azurin to form complexes with the tumor suppressor protein p53 and enhance its stability was earlier reported from glycerol gradient centrifugation and GST pull-down assays (*3*, *4*). Using isothermal titration calorimetry, Apiyo and Wittung-Stafshede (*43*) recently demonstrated that four azurin molecules bind per p53 monomer and that azurin binds to p53 with a K_d value of 33 ± 12 nM per site. They further concluded that azurin binds to the N-terminal domain of p53 via its hydrophobic patch and likely competes with MDM2 binding because azurin's affinity for p53 is higher than that of MDM2. The competitive displacement of MDM2 explains the stability and higher intracellular accumulation of p53 in p53-positive cancer cells, leading to apoptosis and cell death. The involvement of the hydrophobic patch in p53 binding, which is located in the N-terminal to central region of azurin, agrees with the GST pull-down assays, demonstrating p53 binding with the N-terminal and central domain of azurin (*4*). The central domain of azurin (amino acids 50−77) also contains the protein transduction domain (PTD) that allows the efficient entry of azurin into various cancer cells over normal cells (*6*). In view of the location of the G−H loop in the C-terminal of azurin that allows inhibition of cancer cell progression through interference of the EphB2/ephrinB2 signaling mechanism, it is clear that azurin is well designed to enter preferentially into cancer cells and to cause cancer cell growth arrest by multiple mechanisms. The high affinity of azurin for EphB2 as compared to ephrinB2 acting as an antagonist, is reminiscent of azurin's high affinity for the tumor suppressor p53, allowing competitive displacement of MDM2 (*43*). Because ephrinB2 is also involved in the attachment of Nipah and Hendra viruses for their cellular entry (*20*, *21*), the antagonistic action of the cupredoxins or their G−H loop peptides might be useful in the treatment of such viral infections. Because no physiological function of azurin is known (*6*, *42*), it is tempting to speculate that *P. aeruginosa* uses azurin to suppress cancer cell growth while it is resident in human bodies during its infection. Although attempts are currently being made to design synthetic peptides as antagonists for EphB receptor binding (*33*, *34*), it is interesting to note that such antagonistic peptides with high affinity for the EphB receptors have already been incorporated in some bacterial proteins as a process of natural evolution against cancer progression, that we can hopefully tap into as potential drugs (*44*, *45*).

There are some apparent discrepancies in our data that need an explanation. For example, the K_d values of azurin or GST-Azu 88−113 binding with EphB2 range from 6 to 12 nM (Table 3). Yet, it needs 1 μM or higher amounts to observe their growth inhibiting effects on cancer cells (Figures 7D and 8B). The reason is that the K_d values were determined among interacting proteins in the absence of any other interfering agents. In contrast, when azurin (or its truncated derivatives) is added to growing cells, it can bind other cellular components such as ICAM-3 or DC-SIGN (*46*). Azuin can also enter preferentially into the cancer cells by receptor-mediated endocytosis (*6*) and be engaged in binding the tumor suppressor p53 (*3*, *4*, *43*) so that a major part will not be available to bind with the surface-exposed EphB2 receptors. In addition, azurin can bind other receptors such as A6, A4, and A7 (Figure 2A) and will not be available to bind the EphB2 receptors, explaining why a higher concentration of azurin (or peptides derived from it) is necessary to affect the signaling process and cancer growth. The EphB2/ephrinB2 receptor/ligand is known to be upregulated, and the ensuing signaling promotes growth of breast cancer or prostate cancer cells (*16*, *17*, *41*). Thus, although the EphB2-negative DU145 cells, where the ephrinB2 levels are somewhat reduced (*47*), still grow very well and are not susceptible to growth inhibition by azurin or its truncated derivatives (Figure 8A), the EphB2 transfected cells have a higher growth rate. Azurin, Azu 36−128, or Azu 88−113 peptide inhibits this EphB2-promoted enhanced growth rate (Figure 8B) by interfering in tyrosine phosphorylation (Figure 6A and B) and the consequent signaling process. The tyrosine phosphorylation experiments were conducted in serum-starved cells to keep the background levels low so as to enable the measurement of the inhibitory effect of azurin (Figure 6A) or GST-Azu 88−113 fusion protein (Figure 6B) on cell signaling in EphB2-transfected DU145 cells in the presence of exogenous ephrinB2. The fact that there are 16 Eph receptor tyrosine kinases and 9 ephrins producing various levels of phosphorylated tyrosine during active growth of cancer cells makes it difficult to measure the level of inhibition of EphB2/ephrinB2-mediated tyrosine phosphorylation during the active growth stage as shown in Figures 7D or 8B, and such experiments were, therefore, conducted in serum-starved cells as shown in Figure 6.

REFERENCES

1. De Rienzo, F., Gabdoulline, R. R., Menziani, M. C., and Wade, R. C. (2000) Blue copper proteins: a comparative analysis of their molecular interaction properties, *Protein Sci. 9*, 1439−1454.
2. Murphy, L. M., Dodd, F. E., Yousafzai, F. K., Eady, R. R., and Hasnain, S. S. (2002) Electron donation between copper containing nitrite reductases and cupredoxins: the nature of protein-protein interaction in complex formation, *J. Mol. Biol. 315*, 859−871.

3. Yamada, T., Goto, M., Punj, V., Zaborina, O., Chen, M. L., Kimbara, K., Majumdar, D., Cunningham, E., Das, Gupta, T. K., and Chakrabarty, A. M. (2002) Bacterial redox protein azurin, tumor suppressor protein p53, and regression of cancer, *Proc. Natl. Acad. Sci. U.S.A. 99*, 14098−14103.
4. Punj, V., Bhattacharyya, S., Saint-Dic, D., Vasu, C., Cunningham, E. A., Graves, J., Yamada, T., Constantinou, AI., Christov, K., White, B., Li, G., Majumdar, D., Chakrabarty, A. M., and Das, Gupta, T. K. (2004) Bacterial cupredoxin azurin as an inducer of apoptosis and regression in human breast cancer, *Oncogene 23*, 2367−2378.
5. Yamada, T., Hiraoka, Y., Das, Gupta, T. K., and Chakrabarty, A. M. (2004) Rusticyanin, a bacterial electron transfer protein, causes G1 arrest in J774 and apoptosis in human cancer cells, *Cell Cycle 3*, 1182−1187.
6. Yamada, T., Fialho, A. M., Punj, V., Bratescu, L., Das, Gupta, T. K., and Chakrabarty, A. M. (2005) Internalization of bacterial redox protein azurin in mammalian cells: entry domain and specificity, *Cell. Microbiol. 7*, 1418−1431.
7. Yamada, T., Hiraoka, Y., Ikehata, M., Kimbara, K, Avner, B. S., Das, Gupta, T. K., and Chakrabarty, A. M. (2004) Apoptosis or growth arrest: Modulation of tumor suppressor p53's specificity by bacterial redox protein azurin, *Proc. Natl. Acad. Sci. U.S.A. 101*, 4770−4775.
8. Gough, J., and Chothia, C. (2004) The linked conservation of structure and function in a family of high diversity: the monomeric cupredoxins, *Structure 12*, 917−925.
9. Himanen, J. P., Rajashankar, K. R., Lackmann, M., Cowan, C. A., Henkemeyer, M., and Nikolov, D. B. (2001) Crystal structure of an Eph receptor-ephrin complex, *Nature 414*, 933−938.
10. Toth, J., Cutforth, T., Gelinas, A. D., Bethney, K. A., Bard, J. and Harrison, C. J. (2001) Crystal structure of an ephrin ectodomain, *Dev. Cell 1*, 83−92.
11. Nikolov, D. B., Li, C., Barton, W. A., and Himanen, J. P. (2005) Crystal structure of the ephrin-B1 ectodomain: implications for receptor recognition and signaling, *Biochemistry 44*, 10947−10953.
12. Blits-Huizinga, C. T., Nelersa, C. M, Malhotra, A. and Liebl, D. J. (2004) Ephrins and their receptors: binding versus biology, *IUBMB Life 56*, 257−265.
13. Hafner, C., Schmitz, G., Meyer, S., Bataille, F., Hau, P., Langmann, T., Dietmaier, W., Landthaler, M., and Vogt, T. (2004) Differential gene expression of Eph receptors and ephrins in benign human tissues and cancers, *Clin. Chem. 50*, 490−499.
14. Nakada, M., Niska, J. A., Miyamori, H., McDonough, W. S., Wu, J., Sato, H., and Berens, M. E. (2004) The phosphorylation of EphB2 receptor regulates migration and invasion of human glioma cells, *Cancer Res. 64*, 3179−3185.
15. Lugli, A., Spichtin, H., Maurer, R., Mirlacher, M., Kiefer, J., Huusko, P., Azorsa, D., Terracciano, L., Sauter, G., Kallioniemi, O. P., Mouses, S., and Tornillo, L. (2005) EphB2 expression across 138 human tumor types in a tissue microarray: high levels of expression in gastrointestinal cancers, *Clin. Cancer Res. 11*, 6450−6458.
16. Kittles, R. A., Boffoe-Bonnie, A., Moses, T., Robbins, C., Ahaghotu, C., Huusko, P., Pettaway, C., Vijayakumar, S., Bennett, J., Hoke, G., Mason, T., Weinrich, S., Trent, J, Collins, F., Mousses, S., Bailey-Wilson, J., Furbert-Harris, P., Dunston, G., Powell, I., and Carpten, J. D. (2006) A common nonsense mutation in EphB2 is associated with prostate cancer risk in African American men with a positive family history, *J. Med. Genet. 43*, 507−511.
17. Surawska, H., Ma, P. C., and Salgia, R. (2004) The role of ephrins and Eph receptors in cancer, *Cytokine Growth Factor Rev. 15*, 419−433.
18. Brantley-Sieders, D. M., and Chen, J. (2004) Eph receptor tyrosine kinases in angiogenesis: from development to disease, *Angiogenesis 7*, 17−28.
19. Wimmer-Kleikamp, S. H., and Lackmann, M. (2005) Eph-modulated cell morphology, adhesion and motility in carcinogenesis, *IUBMB Life 57*, 421−431.
20. Bonaparte, M. I., Dimitrov, A. S., Bossart, K. N., Crameri, G., Mungal, B. A., Bishop, K. A., Choudhry, V., Dimitrov, D. S., Wang, L.-F., Eaton, B. T. and Broder, C. C. (2005) Ephrin-B2 ligand is a functional receptor for Hendra virus and Nipah virus, *Proc. Natl. Acad. Sci. U.S.A. 102*, 10652−10657.
21. Negrete, O. A., Levroney, E. L., Aguilar, H. C., Bertolotti-Ciarlet, A., Nazarian, R., Tajyar, S., and Lee, B. (2005) EphrinB2 is the entry receptor for Nipah virus, an emergent deadly paramyxovirus, *Nature 436*, 401−405.
22. Hiraoka, Y., Yamada, T., Goto, M., Das, Gupta, T. K., and Chakrabarty, A. M. (2004) Modulation of mammalian cell growth and death by prokaryotic and eukaryotic cytochrome c, *Proc. Natl. Acad. Sci. U.S.A. 101*, 6427−6432.
23. Schlarb, B. G., Wagner, M. J., Vijgenboom, E., Ubbink, M., Bendall, D. S., and Howe, C. J. (1999) Expression of plastocyanin and cytochrome f of the cyanobacterium Phormidium laminosum in Escherichia coli and Paracoccus denitrificans and the role of leader peptides, *Gene 234*, 275−283.
24. Mosmann, T. (1983) Rapid colorimetric assay for cellular growth and survival: application to proliferation and cytotoxicity assays, *J. Immunol. Methods 65*, 55−63.
25. Holm, L., and Sander, C. (1993) Protein structure comparison by alignment of distance matrices, *J. Mol. Biol. 233*, 123−138.
26. Gibrat, J. F., Madej, J., and Bryant, S. H., (1996) Surprising similarities in structure comparison, *Curr. Opin. Struct. Biol. 6*, 377−385.
27. Torrance, G. M., Gilbert, D. R., Michalopoulos, I., and Westhead, D. W. (2005) Protein structure topological comparison, discovery and matching service, *Bioinformatics 21*, 2537−2538.
28. Koradi, R., Billeter, M., and Wuthrich, K. (1996) MOLMOL: a program for display and analysis of macromolecular structures, *J. Mol. Graphics 14*, 51−55.
29. Himanen, J. P., Chumley, M. J., Lackmann, M., Li, C., Barton, W. A., Jeffrey, P. D., Vearing, C., et al. (2004) Repelling class discrimination: ephrin-A5 binds to and activates EphB2 receptor signaling, *Nat. Neurosci. 7*, 501−509.
30. Pasquale, E. B. (2004) Eph-ephrin promiscuity is now crystal clear, *Nat. Neurosci. 7*, 417−418.
31. Huusko, P., Ponciano-Jackson, D., Wolf, M., Kiefer, J. A., Azorsa, D. O., Weaver, D., et. al. (2004) Nonsense-mediated decay microarray analysis identifies mutations of EPHB2 in human prostate cancer, *Nat. Genet. 36*, 979−983.
32. Mao, W., Luis, E., Ross, S., Silva, J., Tan, C., Crowley, C., Chui, C., Franz, G., Senter, P., Koeppen, H., and Polakis, P. (2004) EphB2 as a therapeutic antibody drug target for the treatment of colorectal cancer, *Cancer Res. 64*, 781−788.
33. Murai, K. K., Nguyen, L. N., Koolpe, M., McLennan, R., Krull, C. E., and Pasquale, E. B. (2003) Targeting the EphA4 receptor in the nervous system with biologically active peptides, *Mol. Cell. Neurosci. 24*, 1000−1011.
34. Koolpe, M., Burgess, R., Dail, M., and Pasquale, E. B. (2005) EphB receptor-binding peptides identified by phage display enable design of an antagonist with ephrin-like affinity, *J. Biol. Chem. 280*, 17301−17311.
35. Torchilin, V. P., and Lukyanov, A. N. (2003) Peptide and protein drug delivery to and into tumors: challenges and solutions, *Drug Discovery Today 8*, 259−266.
36. Sa-Correia, I., Fialho, A. M., Videira, P. A., Moreira, L. M., Marques, A. R., and Albano, H. (2002) Gellan gum biosynthesis in Sphingomonas paucimobilis ATCC 31461: genes, enzymes and exopolysaccharide production engineering, *J. Ind. Microbiol. Biotechnol. 28*, 170−176.
37. Mukai-Correa, R., Prata, A. S., Alvim, I. D., and Grosso, C. R. (2004) Controlled release of protein from hydrocolloid gel microbeads before and after drying, *Curr. Drug Delivery 1*, 265.
38. Brambilla, R., and Klein, R. (1995) Telling axons where to grow: a role for Eph receptor tyrosine kinases in guidance, *Mol. Cell. Neurosci. 6*, 487−495.
39. Adams, R. H., Wilkinson, G. A., Weiss, C. C., Diella, F., Gale, N. W., Deutsch, U., Risau, W. and Klein, R. (1999) Roles of ephrinB ligands and EphB receptors in cardiovascular development: demarcation of arterial/venous domains, vascular morphogenesis, and sprouting angiogenesis, *Genes Dev. 13*, 295−306.
40. Katakowski, M., Zhang, Z., de Carvalho, A. C., and Chopp, M. (2005) EphB2 induces proliferation and promotes a neuronal fate in adult subventricular neural precursor cells, *Neurosci. Lett. 385*, 204−209.
41. Wu, Q., Suo, Z., Risberg, B., Karlsson, M. G., Villman, K., and Nesland, J. M. (2004) Expression of Ephb2 and Ephb4 in breast carcinoma, *Pathol. Oncol. Res. 10*, 26−33.
42. Vijgenboom, E., Busch, J. E., and Canters, G. W. (1997) In vivo studies disprove an obligatory role of azurin in denitrification in

Pseudomonas aeruginosa and show that azu expression is under control of RpoS and ANR, *Microbiology 143*, 2853−2863.
43. Apiyo, D., and Wittung-Stafshede, P. (2005) Unique complex between bacterial azurin and tumor-suppressor protein p53, *Biochem. Biophys. Res. Commun. 332*, 965−968.
44. Fialho, A. M., Das Gupta, T. K., and Chakrabarty, A. M. (2007) Designing promiscuous drugs? Look at what nature made! *Lett. Drug Des. Discovery 4*, 40−43.
45. Mahfouz, M., Hashimoto, W., Das Gupta, T. K., and Chakrabarty, A. M. (2007) Bacterial proteins and CpG-rich extrachromosomal DNA in potential cancer therapy, *Plasmid 57*, 4−17.
46. Chaudhari, A., Fialho, A. M., Ratner, D., Gupta, P., Hong, C. S., Kahali, S., Yamada, T., Haldar, K., Murphy, S., et al. (2006) Azurin, Plasmodium falciparum malaria and HIV/AIDS: inhibition of parasitic and viral growth by azurin, *Cell Cycle 5*, 1642−1648.
47. Fox, B. P., Tabone, C. J., and Kandpal, R. P. (2006) Potential clinical relevance of Eph receptors and ephrin ligands expressed in prostate carcinoma cell lines, *Biochem. Biophys. Res. Commun. 342*, 1263−1272.

BI061661X